Journal of Biomechanics 73 (2018) 9–17

Contents lists available at ScienceDirect

Journal of Biomechanics

journal homepage: www.elsevier.com/locate/jbiomech
www.JBiomech.com

Understanding the relationship between cell death and tissue shrinkage via a stochastic agent-based model

E. Lejeune, C. Linder *

Department of Civil and Environmental Engineering, Stanford University, Stanford, CA 94305, USA

ARTICLE INFO

Article history:
Accepted 8 March 2018

Keywords:
Agent-based model
Cell death
Sensitivity analysis
Tissue shrinkage
Multi-scale model

ABSTRACT

Cell death, a process which can occur both naturally and in response to insult, is both a complex and diverse phenomenon. Under some circumstances, dying cells actively contract and cause their neighbors to rearrange and maintain tissue integrity. Under other circumstances, dying cells leave behind gaps, which results in tissue separation. A better understanding of how the cellular scale features of cell death manifest on the population scale has implications ranging from morphogenesis to tumor response to treatment. However, the mechanistic relationship between cell death and population scale shrinkage is not well understood, and computational methods for studying these relationships are not well established. Here we propose a mechanically robust agent-based cell model designed to capture the implications of cell death on the population scale. In our agent-based model, algorithmic rules applied on the cellular level emerge on the population scale where their effects are quantified. To better quantify model uncertainty and parameter interactions, we implement a recently developed technique for conducting a variance-based sensitivity analysis on the stochastic model. From this analysis and subsequent investigation, we find that cellular scale shrinkage has the largest influence of all model parameters tested, and that by adjusting cellular scale shrinkage population shrinkage varies widely even across simulations which contain the same fraction of dying cells. We anticipate that the methods and results presented here are a starting point for significant future investigation toward quantifying the implications of different mechanisms of cell death on population and tissue scale behavior.

1. Introduction

Cell death is fundamental to multi-cellular systems. Apoptosis, or programmed cell death, is required for both organ development (Suzanne and Steller, 2013; Monier and Suzanne, 2015) and for maintaining tissue homeostasis (Renehan et al., 2001). For example, programmed cell death is know to be an important part of digit formation (Hernández-Martínez and Covarrubias, 2011), dorsal closure during Drosophilia embryogenesis (Toyama et al., 2008), and epithelial folding (Monier et al., 2015). Notably, in some circumstances cell death leads to tissue closure and maintenance of tissue integrity, while in other circumstances cell death leads to tissue splitting apart and separating (Suzanne and Steller, 2013). Beyond physiological function, cancer treatments such as radiation therapy are intended to shrink tumors by inducing cell death in targeted tissue (Baskar et al., 2012; Cohen-Jonathan et al., 1999). However, connecting macroscale tumor shrinkage to cellular scale death is not necessarily straightforward. As evidenced by the multiple roles of cell death in physiological function, cell death is a complex and diverse phenomenon. Here, we establish a framework and run initial tests toward connecting instances of cellular scale death to population and tissue scale shrinkage through a stochastic agent-based modeling framework, illustrated in Fig. 1.

Modeling tumor response to intervention is a highly active area of research (Ribba et al., 2012; Angeli and Stylianopoulos, 2016). On the tissue scale, it is too computationally expensive to explicitly model every single individual cell and all of their interactions. One approach to handling this limitation is to capture the components of a tumor phenomenologically through a system of partial differential equations (Lima et al., 2015). Another strategy is to create a multi-scale framework and couple a cellular scale model, where cells are represented explicitly, with a continuum scale representation (Rahman et al., 2017). Although cell death is frequently implemented in these models (Titz and Jeraj, 2008; Zacharaki et al., 2004), either explicitly or phenomenologically, open questions remain towards quantifying the relationship between cell death mechanism and tissue scale shrinkage. In this paper, we consider two main types of cell death, illustrated in Fig. 1. First, passive cell

* Corresponding author at: 473 Via Ortega, Stanford, CA 94305, USA.
E-mail address: linder@stanford.edu (C. Linder).

https://doi.org/10.1016/j.jbiomech.2018.03.019
0021-9290/

death, often called "necrosis", which involves cell membrane rupture and release of cell contents (Berghe et al., 2014). Second, active cell death, often referred to as "apoptosis" or "programmed cell death", where the cell contracts and breaks into several apoptotic bodies (Elmore, 2007). Notably, apoptosis is typically associated with a decrease in cell volume, referred to here as "cell shrinkage" (Bortner and Cidlowski, 2002). Here we show that there is an important relationship between cell shrinkage during cell death, and population scale deformation induced by cell death. We anticipate that our proposed framework and simulation results will inform future investigation.

The remainder of the paper is organized as follows. In Section 2, we introduce our mechanically driven agent-based model. In Section 3, we motivate and outline the procedure for conducting a sensitivity analysis for our stochastic agent-based model. In Section 4.1 we present the results of the sensitivity analysis, and in Section 4.2 we present some representative parameter sweeps. Finally, we conclude in Section 5.

2. Methods: agent-based model

Agent-based models are a natural starting point for capturing the behavior of biological tissue because the effects of rules and parameters applied on the cellular scale can freely emerge on the population scale (An et al., 2009). In this Section, we introduce a mechanically focused agent-based model specifically designed to capture the cell rearrangements caused by cell death that lead to population scale shrinkage. In Section 2.1, we describe the details of our agent-based model, and in Section 2.2 we describe our post processing technique for computing average population deformation from the position change of each agent throughout the simulation.

2.1. Mechanical model and algorithmic cellular scale mechanisms

The mechanical component of our agent-based model is based on peridynamics, a theoretical and computational framework that is an alternative to classical continuum mechanics and can be implemented numerically as a mesh-free method (Silling, 2000; Silling and Askari, 2005). In this mechanical framework, cells interact with their neighbors as defined by their horizon $\mathcal{H}$, and dual-horizon $\mathcal{H}'$. To define $\mathcal{H}$ and $\mathcal{H}'$ we first define distance δ^* (Ren et al., 2016; Lejeune and Linder, 2017b). For cell j distance δ_j^* is a function of baseline cell interaction distance δ, cell growth g_j, and cell radius r_0 written as

$$\delta_j^* = 2(1+g_j)\,\delta_j\, r_0. \tag{1}$$

With this definition of δ^*, the horizon of node j $\mathcal{H}_j$ is defined by cell position in the current configuration $\boldsymbol{y}_j$ and $\boldsymbol{y}_k$ as

$$\mathcal{H}_j = \{k \mid \quad \|\boldsymbol{y}_j - \boldsymbol{y}_k\| \; < \; \delta_j^*\}. \tag{2}$$

Using this definition, the dual-horizon $\mathcal{H}'_j$ is defined as

$$\mathcal{H}'_j = \{k \mid \quad j \in \mathcal{H}_k\}. \tag{3}$$

Cells j and k interact when the distance between them, defined by position in the current configuration $\boldsymbol{y}_j$ and $\boldsymbol{y}_k$ is less than either δ_j^* or δ_k^*. This interaction is formalized through the dual-horizon peridynamics equation of motion written in the discrete form as

$$0 = \sum_{k\in\mathcal{H}'_j} \boldsymbol{f}_{jk}(\boldsymbol{y}_j,\boldsymbol{y}_k)\,\Delta V_k - \sum_{k\in\mathcal{H}_j} \boldsymbol{f}_{kj}(\boldsymbol{y}_j,\boldsymbol{y}_k)\,\Delta V_k \tag{4}$$

for static equilibrium in the absence of body forces, where $\boldsymbol{f}_{jk}$ is force density acting at j due to k, $\boldsymbol{f}_{kj}$ is force density acting at k due to j, and ΔV is volume (Ren et al., 2016). Consistent with previous work, here we choose a state-based peridynamic linear elastic solid with a growth term as the constitutive law for computing $\boldsymbol{f}$. Growth term g is defined as radial growth of a cell such that current cell radius r^t is a function of initial cell radius r_0 and g^t as

$$r^t = (1+g^t)\,r_0. \tag{5}$$

Further details of model implementation including the implementation of the constitutive law are found in Appendix A and Lejeune and Linder (2017b). We also note that the cells are formulated as three-dimensional deformable objects, though here we restrict the motion of cell centers to the two-dimensional plane.

In addition to the purely mechanical components of our model, we implement algorithmic rules to capture cellular scale behavior. Due to practical limitations, it is not feasible to include all potential cell behavior in a single model, rather researchers must take a pragmatic approach (Jagiella et al., 2016). In constructing this model, we focus exclusively on cell shrinkage and cell death, in contrast to prior model implementations which focus on cell growth and proliferation (Lejeune and Linder, 2017a). We start with an initial population of cells, and when the simulation begins a certain fraction of cells undergo the cell death process. The simulation is complete when the cell death process is complete in all of the cells where it was triggered.

In these simulations, we consider two types of uncertainty. First, we treat some of the parameter values that enter the model as unknown. These parameters are sources of epistemic uncertainty. Second, because cellular behavior is inherently stochastic, we must explicitly define sources of aleatoric uncertainty in our simulations (Boon et al., 2016; Yan et al., 2010). When conducting a sensitivity analysis, as described in Section 3, this distinction between epistemic and aleatoric uncertainty is critical. For this initial model, we define three representative sources of epistemic uncertainty, known from experience to have some degree of influence on simulation results. We consider baseline cell interaction distance δ, cell shrinkage α, and the standard deviation of initial cell size distribution β.

First, we consider parameter δ from Eq. (1). The lower bound of δ is defined as $\delta > 1$ because this guarantees that cells will interact with their immediate neighbors and detect new neighbors as cells rearrange. The upper bound of δ is defined such that forces will not build up directly between cells beyond immediate neighbors. The plausible upper bound for δ is set at $\delta = 1.15$ based on experience with the specific model detailed in Appendix A.

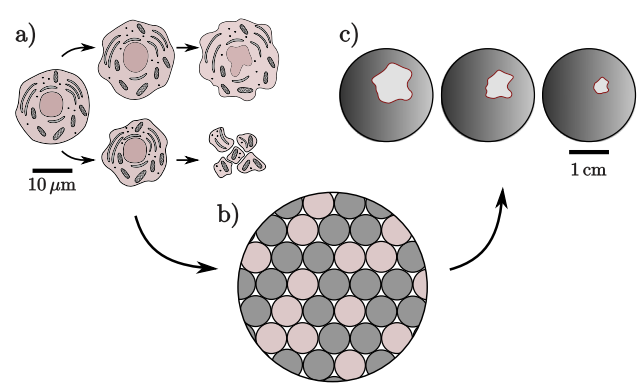

Fig. 1. (a) There are multiple different types of cell death. Illustrated in the upper row, cell death follows a pattern of passive cell death often referred to as "necrosis" where the cell membrane loses integrity. In the lower row, the cell undergoes "apoptosis" where it shrinks and condenses significantly before degrading into small apoptotic bodies; (b) agent-based population scale model of cells where some cells undergo cell death; (c) on the macroscale, cell death manifests as tissue shrinkage, for example in a tumor undergoing radiation therapy. The agent-based model (b) is used to connect the mechanisms depicted in (a) to the tissue scale phenomena illustrated in (c).

Next, we consider that cell death may involve substantial cell shrinkage. In this paper, we adopt the idea of an "apoptosis-necrosis continuum" (Zeiss, 2003) where we primarily distinguish between types of cell death through a cell shrinkage parameter referred to as α. In our model, α corresponds to the amount that a cell shrinks before it stops influencing its neighbors. In the numerical setting, radial shrinkage occurs incrementally where $g_{\text{inc}} < 0$ is applied as

$$g^{t+1} = (1 + g^t)(1 + g_{\text{inc}}) - 1. \tag{6}$$

Essentially, a dying cell will shrink until it reaches a size controlled by α where it will be effectively deleted from the simulation and stop influencing its neighbors. Cell removal is triggered when

$$\frac{r_i}{r_0} = \frac{(1 + g_i)\, r_0}{r_0} < \alpha. \tag{7}$$

Therefore, $\alpha = 1$ corresponds to a perfectly passive cell death while $\alpha < 1$ corresponds to an active cell death, with smaller α a more active process. Our simplified version of cell death is illustrated in Fig. 2a. In the sensitivity analysis, the value of α is considered a source of epistemic uncertainty.

Rather than starting the simulation with cells all of an identical size such that all cells die perfectly in sync, initial cell volume is randomly distributed uniformly between V_0 and $(1 + \beta)V_0$. This is done by assigning an initial amount of growth to each cell as

$$\omega \sim \mathcal{U}(0, 1) \qquad g_0 = \sqrt[3]{\omega\beta + 1} - 1. \tag{8}$$

The consequence of this initial condition is illustrated in Fig. 2b. In the sensitivity analysis, the value of β is a source of epistemic uncertainty, while the stochastic uniform distribution of initial size is a source of aleatoric uncertainty.

When we conduct our sensitivity analysis, we treat the number of cells that die as neither an uncertain nor a stochastic parameter. This is because for our model the relationship between the number of dying cells and population shrinkage is quite intuitive: the more cells that die, the more the population will shrink. As illustrated in Fig. 2c, we assign a set number of cells to shrink but the chosen combination of cells that shrink is determined randomly and is another source of aleatoric uncertainty. In a more complex multi-physics model, the number of dying cells may be controlled by a complex nonlinear relationship worthy of in depth analysis. The parameter ranges used in the sensitivity analysis described in Section 3 are given in Table 1. After performing the sensitivity analysis, we quantify the relationship between number of dying cells and population scale shrinkage in Section 4.2 for sample parameter combinations of δ, α, and β. For both the sensitivity analysis and parameter sweep, repeated runs of the stochastic simulation are required. To readily interpret the results of several thousand simulations we define a post processing technique in Section 2.2.

Table 1
Parameter ranges used for the sensitivity analysis. Uniform parameter distribution is assumed. These parameters were chosen as sources of epistemic uncertainty because they have an unknown influence on model results.

Parameter	Range
horizon δ, Eq. (2)	1.01–1.15
shrinkage α, Eq. (7)	0.3–1.0
initial size β, Eq. (8)	0.0–1.0

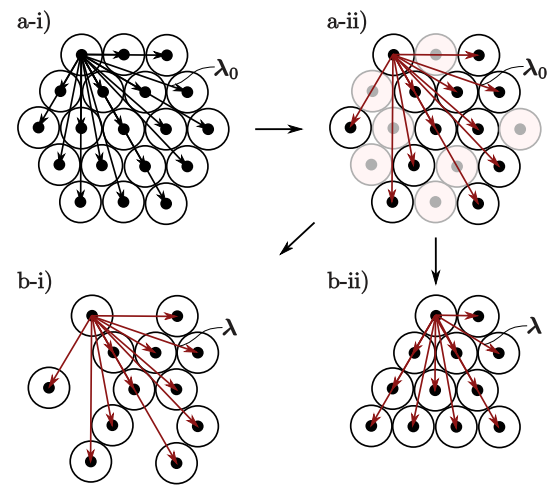

Fig. 3. To compute approximate deformation gradient $\boldsymbol{F}$ from an agent-based simulation with Eq. (11), the positions of cells at the start and end of a simulation are tracked. As illustrated in (a-i), the λ_0 vectors initially connect all cells, but only the vectors connecting cells that are present at both the start and end of the simulation illustrated in (a-ii) are used to build $\boldsymbol{\Lambda}_0$ and $\boldsymbol{\Lambda}$. Different cell configurations for example (b-i) and (b-ii) will lead to different $\boldsymbol{F}$. In the case of (b-i), $\boldsymbol{F}$ will be the identity matrix as the relative positions of nodes does not change.

2.2. Agent-based simulation post-processing

In continuum models designed to capture volumetric growth, growth is often captured via a growth-induced deformation gradient (Ambrosi et al., 2011; Tepole and Kuhl, 2016). Inspired by this paradigm, we develop a technique for summarizing the results of our agent-based models through an approximate deformation gradient (Lejeune and Linder, 2017c). To compute the approximate deformation gradient $\boldsymbol{F}$ in a manner that can accommodate cell death, we define a set of node connectivity vectors $\boldsymbol{\lambda}$ based on the nodes present at the end of the simulation. For the p nodes present

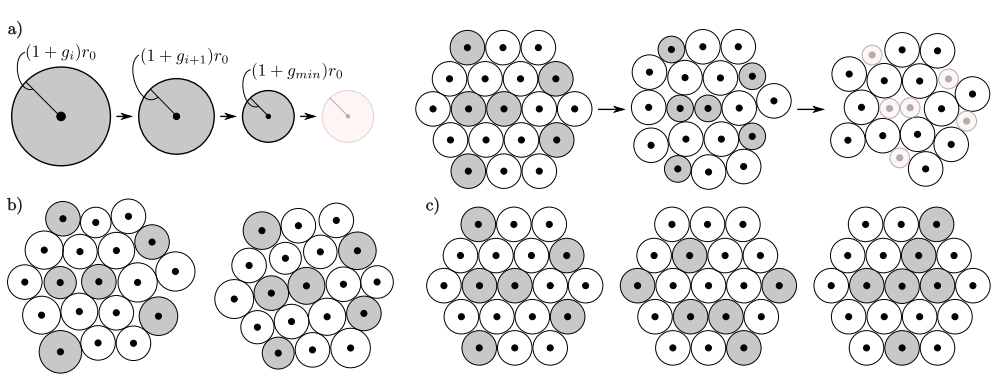

Fig. 2. (a) cell shrinkage and removal when $g = g_{\text{min}} = \alpha$; (b) cells start with randomly perturbed initial size, the range of the perturbation is a source of epistemic uncertainty while the actual values of initial cell size assigned are drawn from a uniform distribution and are a source of aleatoric uncertainty; (c) the combination of cells that shrink is randomly determined, therefore it is a source of aleatoric uncertainty. In our agent-based model, cells are formulated as deformable objects fundamentally described as nodes with an associated preferred radius. In this figure, we visualize cells as circles for simplicity.

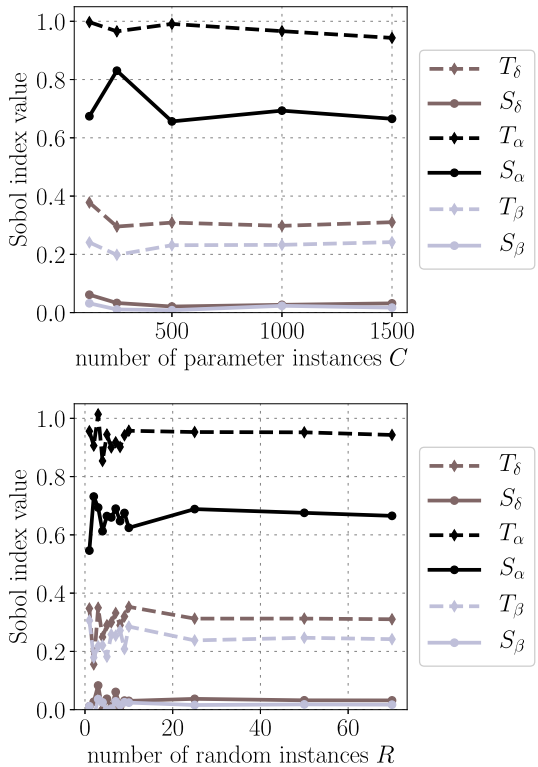

Fig. 4. Upper: convergence with respect to C, $R = 70$. Lower: convergence with respect to R, $C = 1500$. In the sensitivity analysis with $R = 70$ and $C = 1500$, the Sobol indices are as follows: $S_\delta = 0.03$, $S_\alpha = 0.67$, $S_\beta = 0.02$, $T_\delta = 0.31$, $T_\alpha = 0.90$, and $T_\beta = 0.24$. Dummy parameter indices S_γ and T_γ were exactly equal to zero.

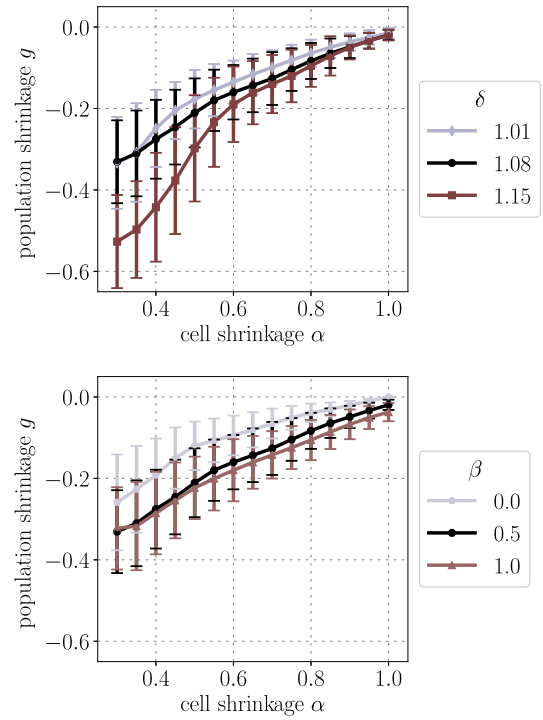

Fig. 5. Upper: population scale shrinkage g with respect to cell shrinkage α with horizon δ varied across curves; Lower: population scale shrinkage g with respect to cell shrinkage α with initial growth distribution β varied across curves. In both plots, lower α corresponds to more population shrinkage while as $\alpha \to 1.0$ less shrinkage occurs the most extreme circumstance occurring at $\beta = 0$ with no population scale shrinkage for $\alpha = 1.0$. Each point corresponds to the average of 200 simulations, and the error bars denote one standard deviation. In all simulations, half of the cells in the population die.

at the end of the simulation, we construct $p(p-1)$ vectors, connecting each node to every other node as illustrated in Fig. 3. Given this connectivity based on nodes present at the end of the simulation, we define an array of initial stretch vectors $\mathbf{\Lambda}_0$ from the position of the nodes at the start of the simulation. We define Λ and Λ_0 as

$$\mathbf{\Lambda}_0 = [\boldsymbol{\lambda}_0^1 \boldsymbol{\lambda}_0^2 \ldots \boldsymbol{\lambda}_0^{p(p-1)}] \qquad \mathbf{\Lambda} = [\boldsymbol{\lambda}^1 \boldsymbol{\lambda}^2 \ldots \boldsymbol{\lambda}^{p(p-1)}]. \tag{9}$$

Given these arrays, we define an approximate average deformation $\boldsymbol{F}$ with the equation

$$\boldsymbol{F}\mathbf{\Lambda}_0 = \mathbf{\Lambda}. \tag{10}$$

To solve this over-determined system of equations (in 2D $\boldsymbol{F}$ is a 2×2 matrix and $\boldsymbol{\lambda}$ is a 2×1 vector), we use the normal equation

$$\boldsymbol{F} = \mathbf{\Lambda}\mathbf{\Lambda}_0^T(\mathbf{\Lambda}_0\mathbf{\Lambda}_0^T)^{-1}. \tag{11}$$

Given this approximate deformation gradient $\boldsymbol{F}$ we can also compute approximate population scale volume change through the Jacobian $J = V/V_0$ and subsequently the macroscale radial population growth g as

$$J = \det \boldsymbol{F} \qquad g = \sqrt{J} - 1. \tag{12}$$

Summarizing the simulation results in a single parameter such as J or g is necessary for the sensitivity analysis procedure discussed in Section 3 where population scale g is chosen as the quantity of interest.

3. Methods: sensitivity analysis

In agent-based computational modeling of biological cells, uncertainty arises due to both lack of knowledge about input parameters (epistemic uncertainty) and the inherently stochastic nature of biological processes on the cellular scale (aleatoric uncertainty) (Oden et al., 2010). Global sensitivity analysis is used to quantify the relationship between proportional uncertainty in model output and the uncertainty in model input (Saltelli, 2004). Classical sensitivity analysis techniques are designed for deterministic models with exclusively epistemic uncertainty. For these techniques to be relevant to highly stochastic models of biological processes, which contain both epistemic and aleatoric uncertainty, additional considerations are often necessary (Gunawan et al., 2005). In Section 3.1, we summarize the general approach for adapting deterministic global sensitivity analysis to the stochastic case. In Section 3.2, we give explicit details for conducting a global sensitivity analysis with the model introduced in Section 2. In Appendix B we provide additional background on our method choice.

3.1. Global sensitivity analysis in a stochastic agent-based model

Sensitivity analysis techniques are well developed for the case without aleatoric uncertainty, where a "black-box" model can be written as $Y = f(\boldsymbol{X})$ where $\boldsymbol{X}$ represents the uncertain input parameters, and Y represents some quantity of interest (Saltelli et al., 2008). Computing Sobol indices, a global variance based sensitivity analysis technique, involves calculating the variance in model output due to a specific model input or a specific combination of model inputs. Sobol indices are defined as

$$S_u = \frac{\mathrm{Var}\{\mathbb{E}\{f(\boldsymbol{X})|\boldsymbol{X}_u\}\}}{\mathrm{Var}\{f(\boldsymbol{X})\}} \qquad u \subset \{1, 2, \ldots, p\} \tag{13}$$

where u is a single parameter or combination of parameters, and S_j with $j \in \{1, 2, \ldots, p\}$ is a first order Sobol index (Sobol, 1993). Total Sobol indices, which sum all first order and higher order interactions from a single parameter j are defined as (Saltelli et al., 2010)

$$T_j = \frac{\mathbb{E}_{\boldsymbol{X}_{\sim j}}\{\mathrm{Var}\{f(\boldsymbol{X})|\boldsymbol{X}_{\sim j}\}\}}{\mathrm{Var}\{f(\boldsymbol{X})\}}. \tag{14}$$

In the numerical setting, strategies for sampling f and computing S_j and T_j are well established (Sobol, 2001; Saltelli, 2002; Saltelli et al., 2010). Here we define models with aleatoric uncertainty as

$$Y = f(\boldsymbol{X}, \omega) \tag{15}$$

where ω represents the aleatoric uncertainty (Hart et al., 2017). In order to conduct a global sensitivity analysis on a stochastic model, we define the model sampling procedure with two quantities: quantity C is the number of model parameter combinations sampled, quantity R is the number of repeated random runs for each parameter combination. To compute the Sobol indices for our stochastic model, we run R sets of C simulations, compute the global sensitivity parameters R times, and then compute the final global sensitivity parameters as the average of R results (Hart et al., 2017). This is discussed further in Appendix B.

3.2. Implementation

In Section 2.1, we defined the sources of epistemic and aleatoric uncertainty in our model. We designed our model such that we are able to compute an instance of aleatoric noise ω prior to running the simulation. This means that we can run the simulation multiple times with different input parameter sets but an identical stochastic component. In many cases, especially with agent-based models, this level of control is not feasible. To deal with this limitation, we recommend two strategies. First, we recommend formulating the agent-based model such that the aleatoric uncertainty is well understood and is as close to reproducible as possible. In some cases, this may be accomplished solely by setting the same random number generation seed for all simulation runs used to compute one set of Sobol indices. Second, acknowledging that perfect control may be impossible, we recommend following the strategy in Marino et al. (2008), and including a dummy parameter in the sensitivity analysis. Essentially, sample values for some dummy parameter γ are computed, the sensitivity analysis is conducting assuming that γ enters the model f even though it does not, and some value is computed for both S_γ and T_γ. Because γ does not actually influence f in any way, any non-zero value of S_γ or T_γ is an artifact. Following Marino et al. (2008), non-zero values of S_γ and T_γ are then treated as a significance threshold. Any parameter in $\boldsymbol{X}$ with a lower index than γ is deemed insignificant. Algorithm 1 summaries our procedure for conducting a sensitivity analysis with our agent-based model from Section 2. The results of our sensitivity analysis are presented in Section 4.1.

Algorithm 1. Sensitivity analysis with a stochastic agent-based population model of cell death. The agent-based model is described in Section 2 and the SALib python library (Herman and Usher, 2017) is used to sample parameters and compute S and T. This algorithm is adapted from Hart et al. (2017).

Input : parameters of interest (δ, α, β) and their ranges, black box stochastic agent-based model for cell death formulated as $f(\delta, \alpha, \beta, \omega)$ where ω is the stochastic component

Output: Distribution and mean of first order Sobol indices and total Sobol indices

Sample: Compute parameter values of δ, α, β, and dummy parameter γ using Saltelli sampling implemented in the SALib python library (`saltelli.sample`). This will result in C samples with different parameter combinations noted as lists δ, α, β, and γ.

Pre-set: Determine R seeds to ensure that the stochastic component ω will be applied in the same way for every combination C when computing one instance of the Sobol indices.

```
for r in 1...R do
    pre-compute the stochastic component for the entire simulation with random seed r as ω(r)
    for c in 1...C do
        run simulation and report approximate growth parameter g as the
        simulation output i.e. if X = [δ[c], α[c], β[c]] compute g = f(X, ω(r)) .
    end
    Compute one instance of the Sobol indices using the results of all C
    simulations and the sobol.analyze function from the SALib python library.
end
Given R values for each Sobol index, compute and report the mean value of each
index S_δ, S_α, S_β, T_δ, T_α, T_β, and dummy parameter indices S_γ and T_γ.
```

4. Results and discussion

The main result of implementing our model is a better understanding of the relationship between the cellular scale interpretation of cell death and population scale shrinkage. In Section 4.1, we present the results of the sensitivity analysis described in Section 3. These results clearly show that in our model uncertainty in cell shrinkage α is the most significant, and that there are non-trivial higher order interactions related to uncertainty in both δ and β. In Section 4.2, we show the effect of varying α for a fixed fraction of dying cells, and the relationship between population scale shrinkage and fraction of dying cells for a fixed set of simulation parameters δ, α, and β.

4.1. Global sensitivity analysis

With the method presented in Section 3, we conduct a global sensitivity analysis and computed the first-order and total Sobol indices for the simulation parameters summarized in Table 1: horizon δ, shrinkage α, and initial size variation β. In all of these simulations, half of the cells in the population die. In this analysis, the quantity of interest is population growth g described in Section 2.2. The results of this analysis are summarized in Fig. 4. When conducting a sensitivity analysis on a deterministic model, it is necessary to check for convergence with respect to the number of parameters sampled C. With a stochastic model, it is necessary to check for convergence with respect to both C and the number repeated stochastic simulations R (Hart et al., 2017). In Fig. 4, we show that we are able to obtain good convergence. At the highest values of C and R tested, we computed $S_\delta = 0.03$, $S_\alpha = 0.67$, $S_\beta = 0.02$, $T_\delta = 0.31$, $T_\alpha = 0.90$, and $T_\beta = 0.24$. When considering just the first-order effects, α appears to be the only significant parameter. However, it is clear from T that both β and δ play a role through higher order interactions. And, as would follow from intuition, shrinkage α is responsible for the highest level of variation in model results. It is worth mentioning that the computational cost of conducting this sensitivity analysis, even for this small number of parameters, was significant both due to the sheer number of simulations required to demonstrate convergence with respect to both C and R, and the non-trivial computational cost of the simulations themselves. Specifically, we ran $R \times C = 105,000$ simulations to demonstrate convergence. In future work, where more parameters and mechanisms will be tested, it will be necessary to develop a computationally cheap surrogate model for an approximate mapping from the simulation input parameters and an instance of noise to g the quantity of interest such that C simulation runs can be conducted using a surrogate model rather than the full computationally expensive simulation. With this work, we set up a point of comparison for future surrogate model development and show results free of conflict regarding the effectiveness of a proposed surrogate modeling technique. Results in Section 4.2 further explore the relationship between δ, α, and β.

4.2. Parameter sweeps

From the results of the sensitivity analysis summarized in Section 4.1, we know that cell shrinkage α is responsible for the majority of the variance in population shrinkage g. In Fig. 5, we show the results of a parameter sweep. We plot g with respect to α for multiple different combinations of δ and β. In both plots, half of the cells in the population undergo cell death. From these curves, it is clear that g varies with respect to α where the least shrinkage $g = 0$ occurs when $\alpha = 1.0$ and $\beta = 0.0$. In the upper plot, where δ varies across curves, it is clear that in general higher δ, or larger cell horizon size, corresponds to more population shrinkage. In the lower plot, where β varies across curves, higher β, or more disparity in initial growth, corresponds to more population shrinkage. Consistent with the results of the sensitivity analysis, the curves show that the influence of δ and β is not trivial. However, in this model, α is the dominant parameter.

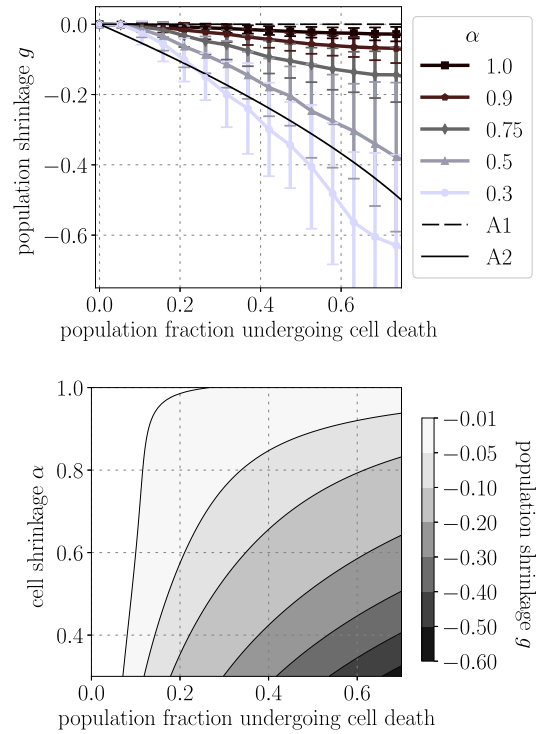

Fig. 6. Upper: Population shrinkage g with respect to the fraction of cells in the population undergoing cell death. Cell shrinkage α varies across curves with horizon $\delta = 1.08$ and initial growth distribution $\beta = 0.5$. As more cells in a population die, g on average decreases. However, g is clearly highly dependent on α. Analytical solution $A1$ (dashed line) shows predicted g if dying cells exert no influence on their neighbors i.e. $g = 0$. Analytical solution $A2$ (solid line) shows predicted g if change in population volume is exactly proportional to the population fraction undergoing cell death d, i.e. $g = \sqrt{1-d} - 1$. In this plot, each point corresponds to the average of 200 simulations, and the error bars denote one standard deviation. Lower: Multivariate adaptive regression splines model of g with respect to d and α for the data shown in the upper plot. The multivariate adaptive regression splines model is fitted using the py-earth package with maximum degree of terms set to 4 and all other terms set to default values (Rudy, 2013; Friedman, 1991).

In all simulations reported thus far, the fraction of cells in the population undergoing cell death is fixed. In every simulation, half of the cells die. This was an appropriate choice for quantifying the influence of α, δ, and β. However, in a real population of dying cells, a more appropriate question is as follows. Given some fraction of cell death, what is the predicted population shrinkage g? In Fig. 6 we present the results of our model reformulated such that g is plotted with respect to the population fraction undergoing cell death. In the upper plot, the different curves show the influence of varying α. In this plot we also show curves A1 and A2 defined as

$$\begin{aligned} A1 &: g = 0 \\ A2 &: g = \sqrt{1-d} - 1 \end{aligned} \tag{16}$$

where d is the population fraction undergoing cell death. Curve A1 shows no change in population volume while curve A2 shows predicted change g if the change in population volume is exactly proportional to the population fraction undergoing cell death. In the most extreme case, where $\alpha = 1.0$, almost no population scale

shrinkage occurs. However, as α decreases so does g such that the overall population shrinkage more than compensates for the loss of volume due to dying cells, implying that the cell shrinkage in fact leads to residual stress in the surviving population. In the lower plot of Fig. 6, we present these simulation results as a contour plot of g with respect to d and α. The contour plot further elucidates the nonlinear relationship between α, d, and g. Although the agent-based model presented here is highly simplified compared to a real biological system, it captures a quite plausible phenomena. Population scale shrinkage due to cell death is dependent on both the number of dying cells and the amount that individual dying cells shrink. Based on these results, it is clear that the mechanism of cell death has significant implications for population scale behavior in both computational models and real biological systems.

5. Conclusion

The main objective of this work was to explore the relationship between cell death and cell population shrinkage and clearly outline a framework for approaching this problem with a stochastic agent-based model. As introduced in Section 1, cell death is a complex and highly variable process. Namely, depending on cell type and circumstance, cell death can exhibit a variety of biochemical and mechanical mechanisms, and can manifest differently on the population and tissue scales. In Section 2, we introduced a mechanically driven agent-based model to capture the effect of cell death on overall population shrinkage. In our model, the interaction distance between cells is controlled by parameter δ, cell shrinkage is controlled by parameter α, and variability in initial cell size is controlled by parameter β. In Section 3, we described a strategy for conducting a sensitivity analysis for our stochastic model. With this technique, we determined that α is the most important parameter for predicting population shrinkage, though the higher order effects associated with δ and β are still significant. The details of our sensitivity analysis are presented in Section 4.1. Finally, our results in Section 4.2 indicate that higher δ and β correspond to more population scale shrinkage, and lower α corresponds to more population scale shrinkage. For a given a set of parameters δ, α, and β a relationship between population shrinkage and fraction of dying cells is established.

Finally, it is worth mentioning that the techniques presented in this paper are quite general. Implementing additional mechanisms in the agent-based model beyond the ones presented in Section 2.1, such as cell migration, the changes in cell stiffness observed during cell death, residual stresses in the cell population prior to the initiation of cell death, dynamic effects, local inflammation, or additional sources of aleatoric uncertainty, would be natural extensions (Nikolaev et al., 2014). Furthermore, the methods put forward in Sections 2.2 and 3 are applicable to alternative cell modeling strategies. Other cell population models that make different assumptions, and potentially overcome some of the limitations of our approach such as the cell-cell interaction algorithm dependent on the position of cell centers rather than cell edges, the simplified representation of cells as a node with an associated radius, and the lack of explicitly implemented tangential forces between cells, can replace the model proposed in Section 2.1 as long as there is a suitable method for tracking the position of cell centers (Pitt-Francis et al., 2009; Van Liedekerke et al., 2018; Sandersius and Newman, 2008). Beyond apoptosis and necrosis, there are a number of additional cell death mechanisms such as "shrinkage necrosis", "oncosis", and "mitotic catastrophe", that are worth exploring (Kerr, 1971; Vakifahmetoglu et al., 2008). Future work within this framework will address creating surrogate models to overcome computational limitations in conducting a sensitivity analysis that includes more parameters, an agent-based model with more potential mechanisms guiding cell behavior, and an extension to the three dimensional case. In addition, future work will involve probing other population scale parameters of interest besides population shrinkage g such as population scale changes in stiffness or average connectivity. Overall, our initial results and methods present a basis for further investigation of the topic.

Conflict of interest

The authors declare no conflict of interest.

Acknowledgements

This work was supported by the National Science Foundation Graduate Research Fellowship under Grant No. DGE-114747.

Appendix A. Agent-based model

In Section 2.1, we introduced the concept of horizon $\mathcal{H}$ and dual-horizon $\mathcal{H}'$ in Eqs. (1)–(3) and the discrete form of the equation of motion in Eq. (4). Here we provide additional background on the state-based peridynamic linear elastic solid with a growth term and the implementation of our model. The notation and methods detailed here are consistent with our prior work and the broader peridynamics literature (Lejeune and Linder, 2017b; Madenci and Oterkus, 2014; Silling and Lehoucq, 2010; Littlewood, 2015; Oterkus, 2015). The continuous form of the peridynamic equation of motion at point $\boldsymbol{x}$ is

$$\rho\ddot{\boldsymbol{u}}(\boldsymbol{x},t) = \int_{\boldsymbol{x}'\in\mathcal{H}'_{\boldsymbol{x}}} \boldsymbol{f}_{\boldsymbol{x}\boldsymbol{x}'}(\boldsymbol{y},\boldsymbol{y}')\,\boldsymbol{d}V_{\boldsymbol{x}'} - \int_{\boldsymbol{x}'\in\mathcal{H}_{\boldsymbol{x}}} \boldsymbol{f}_{\boldsymbol{x}'\boldsymbol{x}}(\boldsymbol{y}',\boldsymbol{y})\,\boldsymbol{d}V_{\boldsymbol{x}'} + \boldsymbol{b}(\boldsymbol{x},t) \tag{A.1}$$

where ρ is density, $\ddot{\boldsymbol{u}}$ is acceleration, $\boldsymbol{x}$ and $\boldsymbol{x}'$ refer to points, t is time, $\mathcal{H}'_{\boldsymbol{x}}$ is the dual-horizon of $\boldsymbol{x}$ defined in Eq. (3), $\mathcal{H}_{\boldsymbol{x}}$ is the horizon of $\boldsymbol{x}$ defined in Eq. (2), $\boldsymbol{f}_{\boldsymbol{x}\boldsymbol{x}'}$ is the force density acting at point $\boldsymbol{x}$ due to $\boldsymbol{x}'$, $\boldsymbol{f}_{\boldsymbol{x}'\boldsymbol{x}}$ is the force density acting at point $\boldsymbol{x}'$ due to $\boldsymbol{x}$, $\boldsymbol{y}$ and $\boldsymbol{y}'$ refer to point positions in the current configuration, V is volume, and $\boldsymbol{b}$ is body force. The discrete form of the equation of motion at static equilibrium with no body force at node j can then be written as

$$0 = \sum_{\mathrm{k}\in\mathcal{H}'_{\mathrm{j}}} \boldsymbol{f}_{\mathrm{jk}}(\boldsymbol{y}_{\mathrm{j}},\boldsymbol{y}_{\mathrm{k}})\,\Delta V_{\mathrm{k}} - \sum_{\mathrm{k}\in\mathcal{H}_{\mathrm{j}}} \boldsymbol{f}_{\mathrm{kj}}(\boldsymbol{y}_{\mathrm{j}},\boldsymbol{y}_{\mathrm{k}})\,\Delta V_{\mathrm{k}} \tag{A.2}$$

which is also reported in Eq. (4). When considering this equation at node j, note that the first term sums over the dual-horizon $\mathcal{H}'_{\mathrm{j}}$ while the second term sums over the horizon $\mathcal{H}_{\mathrm{j}}$. The summation over $\mathcal{H}'_{\mathrm{j}}$ is the summation of all the action forces that arise when nodes k exert force on node j. The summation over $\mathcal{H}_{\mathrm{j}}$ is the summation of all the reaction forces that arise when nodes k receive forces exerted by node j (Ren et al., 2016).

Starting from Eq. (4) in Section 2.1, here we define growth dependent volume as

$$\Delta V_{\mathrm{j}} = (1+g_{\mathrm{j}})^n \Delta V_{\mathrm{j}}^0 \tag{A.3}$$

where g_{j} is the radial growth of cell j and $n = 3$. Then, we formulate the constitutive law that dictates force density $\boldsymbol{f}$. We first define the force-free node separation distance $\|\xi_{\mathrm{jk}}\|$ as

$$\|\xi_{\mathrm{jk}}\| = (1+g_{\mathrm{j}})r_{\mathrm{j}} + (1+g_{\mathrm{k}})r_{\mathrm{k}} \tag{A.4}$$

where r is cell radius. Then, we define the stretch between cells as

$$s_{\mathrm{jk}} = \frac{\|\boldsymbol{y}_{\mathrm{k}} - \boldsymbol{y}_{\mathrm{j}}\| - \|\xi_{\mathrm{jk}}\|}{\|\xi_{\mathrm{jk}}\|} \tag{A.5}$$

where $\boldsymbol{y}$ is position in the current configuration. Then we define bond damage γ as a binary function of stretch

$$\gamma_{jk} = \begin{cases} 1 & \text{if } s < s_{max} \\ 0 & \text{otherwise} \end{cases} \tag{A.6}$$

which in this formulation simply enters the influence function ω as

$$\omega_{jk} = \gamma_{jk}. \tag{A.7}$$

In this implementation, the influence function is simply a constant value. Other strategies, such as an influence function that decays exponentially with respect to distance from the cell center, are also justified. We define horizon weighted volume m as

$$m_j = \sum_{k \in \mathcal{H}_j} \omega_{jk} \|\xi_{jk}\|^2 \Delta V_k. \tag{A.8}$$

We define bond elongation e as

$$e_{jk} = \|\boldsymbol{y}_k - \boldsymbol{y}_j\| - \|\xi_{jk}\|. \tag{A.9}$$

We define dilation θ as

$$\theta_j = \frac{n}{m_j} \sum_{k \in \mathcal{H}_j} \omega_{jk} \|\xi_{jk}\| e_{jk} \Delta V_k. \tag{A.10}$$

We define deviatoric bond elongation e^d as

$$e^d_{jk} = e_{jk} - \frac{\theta_j \|\xi_{jk}\|}{n} \tag{A.11}$$

where $n = 3$ is the dimension. Finally, we define the magnitude of force density that arises at cell k due to cell j as

$$t_{kj} = \frac{n \kappa \theta_j}{m_j} \omega_{jk} \|\xi_{jk}\| + \frac{n(n+2)\mu}{m_j} \omega_{jk} e^d_{jk} \tag{A.12}$$

where κ and μ are Lamé parameters. The term t_{kj} will enter $\mathcal{H}_j$ and $\mathcal{H}'_k$. The magnitude of force density that arises at cell j due to cell k is defined as

$$t_{jk} = \frac{n \kappa \theta_k}{m_k} \omega_{kj} \|\xi_{kj}\| + \frac{n(n+2)\mu}{m_k} \omega_{kj} e^d_{kj}. \tag{A.13}$$

The term t_{jk} will enter $\mathcal{H}'_j$ and $\mathcal{H}_k$. More information of the formulation and notation of state-based peridynamic constitutive laws can be found in (Silling et al., 2007). In Eq. (A.12) and (A.13), we note that even though the equation is formulated as an interaction between two cells, cell-cell interactions throughout $\mathcal{H}_j$ enter through m_j, θ_j, and e^d_{jk}. With the magnitude of force density t defined, the force density vectors that appear in Eq. (4) are finally defined as

$$\begin{aligned} \boldsymbol{f}_{jk}(\boldsymbol{y}_j, \boldsymbol{y}_k) &= t_{jk} \cdot \frac{\boldsymbol{y}_k - \boldsymbol{y}_j}{\|\boldsymbol{y}_k - \boldsymbol{y}_j\|} \\ \boldsymbol{f}_{kj}(\boldsymbol{y}_j, \boldsymbol{y}_k) &= t_{kj} \cdot \frac{-(\boldsymbol{y}_k - \boldsymbol{y}_j)}{\|\boldsymbol{y}_k - \boldsymbol{y}_j\|}. \end{aligned} \tag{A.14}$$

In Table A.1 we list parameters needed to implement the simulation. Numerical implementation of our agent-based model follows from the numerical implementation algorithm in Lejeune and Linder (2017b). In this algorithm, growth (shrinkage) is applied in incremental load steps and the static equilibrium response is computed after each load step using an adaptive dynamic relaxation algorithm (Kilic and Madenci, 2010). The adaptive dynamic relaxation algorithm is used to adjust the position of the nodes to achieve mechanical equilibrium. It is also possible to implement alternative strategies that account for dynamic cell behavior within this framework. In contrast to the original algorithm in Lejeune and Linder (2017b), cell death and subsequent node deletion is implemented rather than cell division and subsequent node generation. In future adaptations of this model, capturing the dynamic response of the population due to cell death will require a different numerical solution algorithm.

Table A.1
This table summarizes the parameters selected for simulation. In Section 4, we report all results in dimensionless form.

Parameter	Value	Source
E	1 kPa	Plausible value
ν	0.45	Nearly incompressible material
r_0	5 μm	Standard value (Drasdo and Höhme, 2005)
s_{tmax}	1.15	Fixed value consistent with previous work (Lejeune and Linder, 2017b)

Appendix B. Sensitivity analysis for stochastic models

At present, there are two main approaches to performing a global sensitivity analysis for stochastic models available in the literature (Marino et al., 2008; Hart et al., 2017). In order to describe these two techniques, we define C as the number of parameter combinations sampled and we define R as the number of repeated stochastic simulation runs with identical parameters. For each random simulation aleatoric uncertainty ω is repeatable between model runs. In other words, for r in $\{1 \ldots R\}$ each simulation c in $\{1 \ldots C\}$ will have identical aleatoric uncertainty unique to r. The first method (chronologically in the literature), referred to as *Method 1*, is as follows (Marino et al., 2008):

1. run R sets of C simulations
2. average all R simulation results so in total there are C mappings from input to average output
3. compute the global sensitivity parameters once

There are several examples of *Method 1* in the literature (Marino et al., 2008; Warsinske et al., 2016; Thiele et al., 2014).

Method 2 reverses the order of Step 2 and Step 3 such that R sets of global sensitivity parameters, S_j and T_j, are computed (Hart et al., 2017):

1. run R sets of C simulations
2. compute the global sensitivity parameters from C simulations R times
3. compute average global sensitivity parameters

Hart et al. (2017) makes the argument that for computing Sobol indices, the order of Step 2 and Step 3 matters, and that *Method 2* is the appropriate choice. With *Method 1*, information is lost when the simulations are averaged. In the main body of this paper, we use *Method 2* because Hart et al. (2017) demonstrated that it is not only the correct approach but also that the two methods are not equivalent.

Table B.1
Comparing *Method 1* and *Method 2* for conducting a sensitivity analysis on a stochastic simulation with $R = 70$ and $C = 1500$.

parameter	*Method 1*	*Method 2*
T_δ	0.08	0.31
S_δ	0.03	0.03
T_α	0.94	0.90
S_α	0.90	0.67
T_β	0.02	0.24
S_β	0.02	0.02
T_γ	0.0	0.0
S_γ	0.0	0.0

In order to corroborate the different results that come from *Method 1* and *Method 2* specifically in the agent-based model setting, we compute T and S with both methods. The results are shown in Table B.1. Clearly, the two methods produce different results especially when computing total Sobol indices T. With *Method 1* the sensitivity of the model to δ and β is lost. From the parameter sweep shown in Fig. 5, this is clearly a poor representation of the model.

References

Ambrosi, D., Ateshian, G., Arruda, E., Cowin, S., Dumais, J., Goriely, A., Holzapfel, G., Humphrey, J., Kemkemer, R., Kuhl, E., et al., 2011. Perspectives on biological growth and remodeling. J. Mech. Phys. Solids 59 (4), 863–883.

An, G., Mi, Q., Dutta-Moscato, J., Vodovotz, Y., 2009. Agent-based models in translational systems biology. Wiley Interdiscipl. Rev.: Syst. Biol. Med. 1 (2), 159–171.

Angeli, S., Stylianopoulos, T., 2016. Biphasic modeling of brain tumor biomechanics and response to radiation treatment. J. Biomech. 49 (9), 1524–1531.

Baskar, R., Lee, K., Yeo, R., Yeoh, K., 2012. Cancer and radiation therapy: current advances and future directions. Int. J. Med. Sci. 9 (3), 193.

Berghe, T., Linkermann, A., Jouan-Lanhouet, S., Walczak, H., Vandenabeele, P., 2014. Regulated necrosis: the expanding network of non-apoptotic cell death pathways. Nat. Rev. Mol. Cell Biol. 15 (2), 135.

Boon, W.M., Koppenol, D.C., Vermolen, F.J., 2016. A multi-agent cell-based model for wound contraction. J. Biomech. 49 (8), 1388–1401.

Bortner, C., Cidlowski, J., 2002. Apoptotic volume decrease and the incredible shrinking cell. Cell Death Differ. 9 (12), 1307.

Cohen-Jonathan, E., Bernhard, E., McKenna, W., 1999. How does radiation kill cells? Curr. Opinion Chem. Biol. 3 (1), 77–83.

Drasdo, D., Höhme, S., 2005. A single-cell-based model of tumor growth in vitro: monolayers and spheroids. Phys. Biol. 2 (3), 133–147.

Elmore, S., 2007. Apoptosis: a review of programmed cell death. Toxicol. Pathol. 35 (4), 495–516.

Friedman, J., 1991. Multivariate adaptive regression splines. Ann. Stat., 1–67

Gunawan, R., Cao, Y., Petzold, L., Doyle, F., 2005. Sensitivity analysis of discrete stochastic systems. Biophys. J. 88 (4), 2530–2540.

Hart, J., Alexanderian, A., Gremaud, P., 2017. Efficient computation of Sobol' indices for stochastic models. SIAM J. Sci. Comput. 39 (4), 1514–1539.

Herman, J., Usher, W., 2017. Salib: an open-source python library for sensitivity analysis. J. Open Source Softw. 2 (9).

Hernández-Martínez, R., Covarrubias, L., 2011. Interdigital cell death function and regulation: new insights on an old programmed cell death model. Develop. Growth Differen. Differen. 53 (2), 245–258.

Jagiella, N., Müller, B., Müller, M., Vignon-Clementel, I., Drasdo, D., 2016. Inferring growth control mechanisms in growing multi-cellular spheroids of NSCLC cells from spatial-temporal image data. PLoS Comput. Biol. 12 (2), 1004412.

Kerr, J., 1971. Shrinkage necrosis: a distinct mode of cellular death. J. Pathol. 105 (1), 13–20.

Kilic, B., Madenci, E., 2010. An adaptive dynamic relaxation method for quasi-static simulations using the peridynamic theory. Theoret. Appl. Fract. Mech. 53 (3), 194–204.

Lejeune, E., Linder, C., 2017a. Modeling mechanical inhomogeneities in small populations of proliferating monolayers and spheroids. Biomech. Model. Mechanobiol. https://doi.org/10.1007/s10237-017-0989-0.

Lejeune, E., Linder, C., 2017b. Modeling tumor growth with peridynamics. Biomech. Model. Mechanobiol., 1–17

Lejeune, E., Linder, C., 2017c. Quantifying the relationship between cell division angle and morphogenesis through computational modeling. J. Theor. Biol. 418, 1–7.

Lima, E., Almeida, R., Oden, J., 2015. Analysis and numerical solution of stochastic phase-field models of tumor growth. Numer. Methods Partial Differen. Eq. 31 (2), 552–574.

Littlewood, D., 2015. Roadmap for Peridynamic Software Implementation. SAND Report. Sandia National Laboratories, Albuquerque, NM and Livermore, CA.

Madenci, E., Oterkus, E., 2014. Peridynamic Theory and its Applications. Springer.

Marino, S., Hogue, I., Ray, C., Kirschner, D., 2008. A methodology for performing global uncertainty and sensitivity analysis in systems biology. J. Theor. Biol. 254 (1), 178–196.

Monier, B., Gettings, M., Gay, G., Mangeat, T., Schott, S., Guarner, A., Suzanne, M., 2015. Apico-basal forces exerted by apoptotic cells drive epithelium folding. Nature 518 (7538), 245.

Monier, B., Suzanne, M., 2015. Chapter twelve-the morphogenetic role of apoptosis. Curr. Top. Develop. Biol. 114, 335–362.

Nikolaev, N.I., Müller, T., Williams, D.J., Liu, Y., 2014. Changes in the stiffness of human mesenchymal stem cells with the progress of cell death as measured by atomic force microscopy. J. Biomech. 47 (3), 625–630.

Oden, T., Moser, R., Ghattas, O., 2010. Computer predictions with quantified uncertainty, part i. SIAM News 43 (9), 1–3.

Oterkus, S., 2015. Peridynamics for the Solution of Multiphysics Problems (Ph.D. thesis). The University of Arizona.

Pitt-Francis, J., Pathmanathan, P., Bernabeu, M., Bordas, R., Cooper, J., Fletcher, A., Mirams, G., Murray, P., Osborne, J., Walter, A., Chapman, S., Garny, A., van Leeuwen, I., Maini, P., Rodriguez, B., Waters, S., Whiteley, J., Byrne, H., Gavaghan, D., 2009. Chaste: a test-driven approach to software development for biological modelling. Comput. Phys. Commun. 180 (12), 2452–2471.

Rahman, M., Feng, Y., Yankeelov, T., Oden, J., 2017. A fully coupled space–time multiscale modeling framework for predicting tumor growth. Comput. Methods Appl. Mech. Eng. 320, 261–286.

Ren, H., Zhuang, X., Cai, Y., Rabczuk, T., 2016. Dual-horizon peridynamics. Int. J. Numer. Meth. Eng. 108 (12), 1451–1476.

Renehan, A., Booth, C., Potten, C., 2001. What is apoptosis, and why is it important? BMJ: Br. Med. J. 322 (7301), 1536.

Ribba, B., Kaloshi, G., Peyre, M., Ricard, D., Calvez, V., Tod, M., Čajavec Bernard, B., Idbaih, A., Psimaras, D., Dainese, L., Pallud, J., 2012. A tumor growth inhibition model for low-grade glioma treated with chemotherapy or radiotherapy. Clin. Cancer Res. 18 (18), 5071–5080.

Rudy, J., 2013. Py–earth 0.1.0. scikit–learn.

Saltelli, A., 2002. Making best use of model evaluations to compute sensitivity indices. Comput. Phys. Commun. 145 (2), 280–297.

Saltelli, A., 2004. Global sensitivity analysis: an introduction. In: Proc. 4th International Conference on Sensitivity Analysis of Model Output, pp. 27–43.

Saltelli, A., Annoni, P., Azzini, I., Campolongo, F., Ratto, M., Tarantola, S., 2010. Variance based sensitivity analysis of model output. Design and estimator for the total sensitivity index. Comput. Phys. Commun. 181 (2), 259–270.

Saltelli, A., Ratto, M., Andres, T., Campolongo, F., Cariboni, J., Gatelli, D., Saisana, M., Tarantola, S., 2008. Global Sensitivity Analysis: The Primer. John Wiley & Sons.

Sandersius, S., Newman, T., 2008. Modeling cell rheology with the subcellular element model. Phys. Biol. 5 (1), 015002.

Silling, S., Askari, E., 2005. A meshfree method based on the peridynamic model of solid mechanics. Comput. Struct. 83 (17), 1526–1535.

Silling, S.A., 2000. Reformulation of elasticity theory for discontinuities and long-range forces. J. Mech. Phys. Solids 48, 175–209.

Silling, S.A., Epton, M., Weckner, O., Xu, J., Askari, E., 2007. Peridynamic states and constitutive modeling. J. Elast. 88 (2), 151–184.

Silling, S.A., Lehoucq, R.B., 2010. Peridynamic theory of solid mechanics. Adv. Appl. Mech. 44, 73–168.

Sobol, I., 1993. Sensitivity estimates for nonlinear mathematical models. Math. Modell. Comput. Exp. 1 (4), 407–414.

Sobol, I., 2001. Global sensitivity indices for nonlinear mathematical models and their monte carlo estimates. Math. Comput. Simul. 55 (1), 271–280.

Suzanne, M., Steller, H., 2013. Shaping organisms with apoptosis. Cell Death Differen. 20 (5), 669.

Tepole, A.B., Kuhl, E., 2016. Computational modeling of chemo-bio-mechanical coupling: a systems-biology approach toward wound healing. Comput. Methods Biomech. Biomed. Eng. 19 (1), 13–30.

Thiele, J., Kurth, W., Grimm, V., 2014. Facilitating parameter estimation and sensitivity analysis of agent-based models: a cookbook using NetLogo and R. J. Artif. Soc. Soc. Simul. 17 (3).

Titz, B., Jeraj, R., 2008. An imaging-based tumour growth and treatment response model: investigating the effect of tumour oxygenation on radiation therapy response. Phys. Med. Biol. 53 (17), 4471.

Toyama, Y., Peralta, X., Wells, A., Kiehart, D., Edwards, G., 2008. Apoptotic force and tissue dynamics during drosophila embryogenesis. Science 321 (5896), 1683–1686.

Vakifahmetoglu, H., Olsson, M., Zhiotovsky, B., 2008. Death through a tragedy: mitotic catastrophe. Cell Death Differen. 15 (7), 1153.

Van Liedekerke, P., Buttenschön, A., Drasdo, D., 2018. Off-lattice agent-based models for cell and tumor growth: Numerical methods implementation, and applications. In: Numerical Methods and Advanced Simulation in Biomechanics and Biological Processes, pp. 245–267.

Warsinske, H., Wheaton, A., Kim, K., Linderman, J., Moore, B., Kirschner, D., 2016. Computational modeling predicts simultaneous targeting of fibroblasts and epithelial cells is necessary for treatment of pulmonary fibrosis. Front. Pharmacol. 7.

Yan, K., Nair, K., Sun, W., 2010. Three dimensional multi-scale modelling and analysis of cell damage in cell-encapsulated alginate constructs. J. Biomech. 43 (6), 1031–1038.

Zacharaki, E., Stamatakos, G., Nikita, K., Uzunoglu, N., 2004. Simulating growth dynamics and radiation response of avascular tumour spheroids—model validation in the case of an emt6/ro multicellular spheroid. Comput. Methods Programs Biomed. 76 (3), 193–206.

Zeiss, C.J., 2003. The apoptosis-necrosis continuum: insights from genetically altered mice. Vet. Pathol. 40 (5), 481–495.